JCTC Journal of Chemical Theory and Computation

Acceleration of Classical Mechanics by Phase Space Constraints

Emilio Martínez-Núñez

Departamento de Química Física, Universidad de Santiago de Compostela, 15782 Santiago de Compostela, Spain

Dmitrii V. Shalashilin*

Physical and Theoretical Chemistry Laboratory, Oxford University, South Parks Road, Oxford OX1 3QZ, U.K.

Received February 7, 2006

Abstract: In this article phase space constrained classical mechanics (PSCCM), a version of accelerated dynamics, is suggested to speed up classical trajectory simulations of slow chemical processes. The approach is based on introducing constraints which lock trajectories in the region of the phase space close to the dividing surface, which separates reactants and products. This results in substantial (up to more than 2 orders of magnitude) speeding up of the trajectory simulation. Actual microcanonical rates are calculated by introducing a correction factor equal to the fraction of the phase volume which is allowed by the constraints. The constraints can be more complex than previously used boosting potentials. The approach has its origin in Intramolecular Dynamics Diffusion Theory, which shows that the majority of nonstatistical effects are localized near the transition state. An excellent agreement with standard trajectory simulation at high energies and Monte Carlo Transition State Theory at low energies is demonstrated for the unimolecular dissociation of methyl nitrite, proving that PSCCM works both in statistical and nonstatistical regimes.

1. Introduction

Speeding up calculations of chemical reaction rates is an important goal of theoretical chemistry. For reactions with a high activation barrier, classical trajectory simulation, which is the most straightforward way to obtain reaction rates, can be very time-consuming even for reactions of moderate sized molecules in the gas phase. Current approaches to speeding up classical trajectory simulations include reduction of degrees of freedom (coarse graining),[1,2] importance sampling of initial conditions near the transition state,[3] and the hyperdynamics approach, which modifies interactions in the system by elevating potential energy wells in order to decrease the reaction barrier[4−8] without changing the characteristics of the transition state. See also ref 9 for some preliminary ideas related to hyperdynamics. Often trajectory simulations[10,11] are performed at temperatures well in excess of those in experiment, and rates are then extrapolated.[12,13]

In this article we introduce and test the method of Phase Space Constrained Classical Dynamics to speed up classical trajectory simulations of low rates of chemical processes. The main idea is to impose constraints which lock trajectories in the region of the phase space close to the dividing surface separating reactants and products (i.e. transition state). This pushes the trajectories toward the dividing surface, thereby decreasing the simulation time and substantially speeding up the trajectory simulation. Actual microcanonical rates are calculated as a product of the accelerated rate and a correction factor equal to the fraction of phase volume allowed by constrains. The justification is provided by Intramolecular Dynamics Diffusion Theory (IDDT),[13−16] which shows that far from the dividing surface the dynamics do not disturb microcanonical distribution so that the majority of nonstatis-

10.1021/ct060042z CCC: $33.50
Published on Web 06/13/2006

tical effects are localized near the transition state. Therefore only the dynamics near the transition state need to be simulated. In the next section we give a brief summary of IDDT and describe the method of Phase Space Constrained Classical Mechanics (PSCCM). In section 3 various implementations of PSCCM are tested for the reaction of dissociation of methyl nitrite ($CH_3ONO \rightarrow CH_3O + NO$). We show that PSCCM reproduces the Monte Carlo Transition State Theory at low energies, where the trajectory rate is statistical, and trajectory simulations which account for nonstatistical effects at high energies. The last section provides a summary and a discussion.

2. Theory

2.1. Trajectory Calculations and Monte Carlo Transition State Theory. The calculation of the microcanonical rate constant $k(E)$ of a chemical reaction begins with choosing a dividing surface, S^*, which separates the reactants and the products in the phase space. Usually S^* is implicitly defined by a critical value of the reaction coordinate $q_r = q_r^*$. The dividing surface can also be defined in the phase space.[17] After that the dynamics of reaction can then be treated either by classical trajectories (CT) or by transition state theory.

In trajectory simulations a microcanonical ensemble of initial phase space points in the region of the reactant is set by a Monte Carlo procedure, which are then propagated in time by numerical integration of Hamilton's equations of motion. The rate can be established by a fit to the first-order rate equation

$$\ln\frac{N(t)}{N(t=0)} = -k^{\mathrm{traj}}(E)t \qquad (1)$$

where N is the number of trajectories still in the region of the reactants.

These trajectory rates can be compared with those obtained by statistical Monte Carlo Transition State Theory (MCTST),[18] which will have the form of a flux through the dividing surface as

$$k^{\mathrm{stat}}(E) = \frac{1}{2}\frac{\int_\Gamma \delta[H(p,q) - E]|\dot{q}_r|\delta(q_r - q_r^*)d\Gamma}{\int_\Gamma \delta[H(p,q) - E]d\Gamma} \qquad (2)$$

The standard numerical approach to MCTST is by the Metropolis random walk.[19] In most cases the computed trajectory rates (1) are lower than those of the purely statistical theory (2), despite the fact that the initial ensemble in the trajectory simulation is microcanonical. This is known as intrinsic non-RRKM behavior.[20,21]

2.2. Brief Summary of IDDT. The Intramolecular Dynamics Diffusional Theory[13−16] was developed to explain and to quantify the intrinsic non-RRKM behavior. IDDT considers only the motion along the reaction coordinate and replaces the Liouville equation of Classical Mechanics by a diffusional equation along this coordinate. The nonstatistical trajectory rates after that can easily be extracted from the rate of diffusion along the reaction coordinate toward the dividing surface (transition state), which serves as an absorbing wall for the diffusion. Initial microcanonical distribution in the reactant region results in the initial statistical rate. However, this initial uniform distribution evolves quickly so that it becomes depleted near the absorbing wall although it remains unchanged (i.e. still microcanonical and uniform) far from the dividing surface. Later the rate of reaction is determined by trajectory diffusion to the depleted region near the adsorbing wall—a process attributed to the intramolecular vibrational energy redistribution (IVR), which cannot be described by transition state theory.

Therefore IDDT predicts that the trajectory rate constant k^{traj} in (1) must be time dependent. By definition the initial ($t=0$) trajectory rate constant must be equal to the statistical k^{stat} given by eq 2. In practice however, this short time rate is never observed in trajectory simulations unless serious efforts are made to detect it.[15,16] The rate observed in trajectory simulations is actually the rate of diffusion along the reaction coordinate toward the dividing surface due to intramolecular vibrational energy redistribution, which is smaller than the initial statistical rate.

$$k^{\mathrm{traj}}(E) = k^{\mathrm{IVR}} < k^{\mathrm{stat}}(E) \qquad (3)$$

Depletion of the distribution near the dividing surface and reduction of the trajectory below the Transition State Theory value k^{stat} is a nonstatistical effect, which becomes stronger as the initial energy increases. At lower energies the rate constant reaches its statistical limit.

$$k^{\mathrm{traj}}(E) \approx k^{\mathrm{stat}}(E) \qquad (4)$$

The energies at which trajectory simulations start yielding statistical results are quite low, and straightforward trajectory simulation is expensive for those energies. Therefore methods of accelerated dynamics are required to reach the statistical limit of classical mechanics. Another conclusion of IDDT, which is important in the context of the present work, is that microcanonical distribution is disturbed only in the vicinity of the dividing surface, which means that all nonstatistical effects are well localized. The IDDT picture has been confirmed by a number of simulations.[13−16]

2.3. Phase Space Constrained Classical Mechanics. As mentioned above, straightforward application of trajectory simulations is extremely time-consuming for energies approaching the activation energy threshold. Calculation of the integrals in the MCTST eq 2 is also difficult. In practice, the δ-function, $\delta(q_r - q_r^*)$, is approximated by a narrow function, which will be nonzero only in the vicinity of the dividing surface. The Monte Carlo random walk only visits the region that contributes to the integral in eq 2 infrequently. This results in a very slow convergence of the MCTST.

An obvious method, which speeds up the convergence of MCTST, has been used in ref 22. It is based on the idea of importance sampling and is illustrated in Figure 1a. The random walk is restricted to the phase volume V_1 close to the dividing surface. The calculated auxiliary rate constant $k_1^{\mathrm{stat}}(E)$ is given by eq 2 with the integral over Γ_1 only. The actual rate can then be calculated by

$$k^{\mathrm{stat}}(E) = k_1^{\mathrm{stat}}(E)\frac{\Gamma_1}{\Gamma} \qquad (5)$$

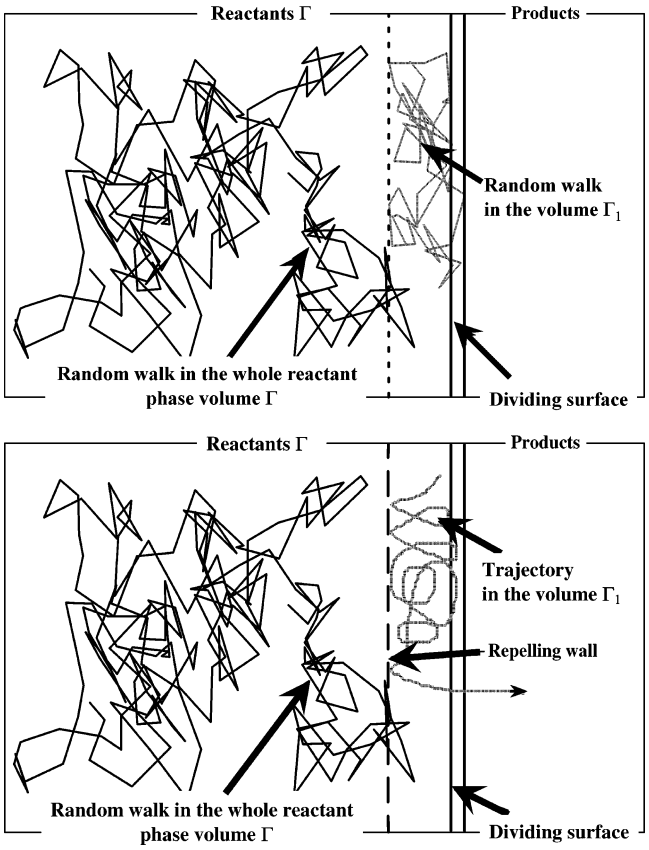

Figure 1. Sketch of the importance sampling approach to Monte Carlo Transition State Theory (frame a) and Phase Space Constrained Classical Mechanics (frame b). In the former the random walk, locked in the volume Γ_1 (dashed line in the frame a), visits the dividing surface more frequently yielding accelerated statistical rate $k_1^{stat}(E)$, while in the latter a trajectory locked in the volume Γ_1 (dashed line in the frame b) crosses the dividing surface and reaches products faster, producing an accelerated trajectory rate $k_1^{traj}(E)$. Both methods require additional random walk (solid line) to calculate the correction factor Γ_1/Γ.

A second random walk is then needed to estimate the volume ratio Γ_1/Γ. This method introduces no new approximations into MCTST but greatly reduces computational time because two short random walks converge much more quickly than a single random walk in the whole phase space.

In this article we propose a method of Phase Space Constrained Classical Mechanics, which expands the technique[22] to trajectory simulations. An outline of the method is illustrated in Figure 1b. The motion of the molecule is restricted in the region close to the dividing surface by applying an auxiliary rigid wall, which repels trajectories in the direction of the products, thus increasing the probability that reactive conditions are reached and dramatically decreasing the cost of the calculation. An analogous expression to eq 5 for the true rate can be defined as

$$k^{traj}(E) = k_1^{traj}(E)\frac{\Gamma_1}{\Gamma} \tag{6}$$

where $k_1^{traj}(E)$ is the accelerated rate constant, and the correction factor Γ_1/Γ is the same as in (5). The advantage of PSCCM in comparison to accelerated MCTST is that PSCCM should be able to take into account nonstatistical intrinsic non-RRKM effects, described by the IDDT.

It should be noted that not only the microcanonical rate constant but also the canonical (i.e. thermal average) rate constant can be estimated using PSCCM. The generalization is not difficult.

The PSCCM method is an application of Importance Sampling, which is well-known within the domain of trajectory simulations. In traditional methods, initial conditions are often biased to the most important region.[3] A new feature of the PSCCM method is the additional biasing of the dynamics itself. The only comparable approach to accelerating classical dynamics is the method suggested by Voter,[4−8] which uses additional "boosting" potentials to push the dynamics toward important regions of the configuration space. There are two advantages of our version of the accelerated dynamics, based on constraints which lock the trajectory in a small portion of the total phase volume rather than on boosting potentials. First, PSCCM relies on a rigorous understanding of nonstatistical effects provided by IDDT, which therefore gives a good idea as to where to put constraints. Second, as will be shown in the next section, phase space constraints can be introduced in a way, which is hard to describe by a boosting potential. It should be also mentioned that phase space constraints were used previously in refs 23−26 for incorporating zero point energy effects into classical mechanics. Although the technique of PSCCM is somewhat similar to that of refs 23−26, our goal is to speed up simulations.

3. Implementation and Test of PSCCM

We have implemented the idea of PSCCM by calculation of the microcanonical rate of dissociation of methyl nitrite (CH_3ONO).

$$CH_3ONO \rightarrow CH_3O + NO \tag{7}$$

3.1. Potential Energy Surface for the Model System. Previously, reaction 7 has been studied both by trajectory simulation and MCTST.[27] For the present study the potential energy surface has been modified in order to prevent another reaction channel considered before,[27] namely

$$CH_3ONO \rightarrow CH_2O + HNO \tag{8}$$

Specifically, the potential energy surface of the present study reads

$$V = V(R_{ON}) + \sum_{i=1}^{5} V(R_i) + \sum_{i=1}^{8} V(\theta_i) + \sum_{i=1}^{4} V(\tau_i) \tag{9}$$

where

$$V(R_{ON}) = D_e\{1 - \exp[-\beta \times (R_{ON} - R_{ON}^{eq})]\}^2 - D_e \tag{10}$$

is the same Morse function as used before[27] but without the switching functions.[27] For the remaining NO, CO, and the three CH bonds the harmonic functions

$$V(R_i) = 0.5K_i^s(R_i - R_i^{eq})^2 \tag{11}$$

Table 1. New Parameters of the Potential Energy Surface Used in the Present Study and Frequencies for *trans*-CH_3ONO

parameter	value (kcal/mol/Å^2)	parameter	value (kcal/mol/Å^2)	parameter	value (kcal/mol/Å^2)
K_{NO}	250	K_{CO}	1250	K_{CH}	650
frequencies					
old PES (ref 27)			this work		
173	931	1459	173	953	1249
246	1049	1670	246	1049	1670
368	1099	2760	372	1103	2807
465	1430	2873	470	1430	2914
715	1430	2909	726	1430	2916

were used to prevent additional dissociation channels. The ONO, CON, HCO, and HCH bending potentials are the same as in ref 27 where they were modeled by the harmonic function

$$V(\theta_i) = 0.5K_i^b(\theta_i - \theta_i^{eq})^2 \quad (12)$$

Finally $V(\tau_i)$ are a cosine series to treat the dihedral interactions in the system (i.e. the CONO and the three HCON dihedrals)

$$V(\tau) = \sum_{i=0}^{5} a_i \cos(i\tau) \quad (13)$$

The parameters of eqs 9−13 are reported in ref 27 except that the force constants of harmonic potentials (11) are used here instead of Morse functions. These K_i^s were adjusted to fit the vibrational frequencies of our previous PES (see Table 1), which was, in turn, developed to reproduce ab initio or experimental (when available) vibrational frequencies, reaction enthalpies, and geometrical parameters. The most crucial parameter is the dissociation energy of the ON bond D_e = 42 kcal/mol which is the same as in ref 27. The vibrational frequencies of *trans*-CH_3ONO (the most stable conformer) are collected in Table 1 together with those calculated with the previous PES.[27] As can be seen the removal of some flexibility in the PES has little effect on the vibrational frequencies of the reactant, and therefore the simplified PES is accurate.

3.2. Trajectory and MCTST Computational Details. Before applying PSCCM we used the new PES to calculate the rate constant by means of standard trajectory simulation (1) and Monte Carlo Transition State Theory (2) in its accelerated version[22] for the following vibrational energies E = 70, 80, 100, and 150 kcal/mol with zero total angular momentum. An extensively modified version of the GENDYN code[11] has been used.

The dividing surface was positioned at the internuclear distance R_{ON}, which minimizes the statistical MCTST reaction rate, namely R_{ON} = 4.3, 3.8, 3.5, and 3.3 Å for E = 70, 80, 100, and 150 kcal/mol, respectively. The minimized MCTST rate constants are collected in Table 2. The accelerated MCTST rate constants were calculated by eq 5 with the restricted phase space volume (Γ_1/Γ) confined to the region between 2 Å and q_r^*. For 80 kcal/mol the calculation of accelerated rates is an order of magnitude faster than by the standard MCTST procedure. For 70 kcal/mol standard MCTST calculations are prohibitive, while accelerated MCTST takes less than 1 h of CPU time. As can be seen in Table 2, the accelerated MCTST rate constants are in very good agreement with the standard calculations, which is not surprising, because the method[22] does not introduce any approximations to MCTST.

Table 2. Accelerated MCTST Rate Constants (in ps^{-1}) Obtained in This Study

energy/(kcal/mol)	q_r^*	accelerated MCTST	standard MCTST
70	4.3	0.000081 ± 0.00002	
80	3.8	0.0012 ± 0.0001	0.0011 ± 0.0001
100	3.5	0.025 ± 0.001	0.025 ± 0.001
150	3.3	0.56 ± 0.02	0.54 ± 0.02

In trajectory simulations, ensembles of 1000 trajectories were employed in all cases (for standard and PSCCM calculations) except for the standard trajectory calculations at 80 kcal/mol, for which we needed 3000 trajectories to achieve the same statistics as in the accelerated computations. In trajectory simulation the dividing surface was chosen to be the same as in the above MCTST (i.e. R_{ON}=4.3, 3.8, 3.5, and 3.3 Å for E=70, 80, 100, and 150 kcal/mol, respectively). Due to a rapid decrease of the rate constant, straightforward trajectory simulation is very slow for E = 80 kcal/mol and is not feasible at all for E = 70 kcal/mol.

3.4. Implementations of the PSCCM Methods. The most straightforward implementation of PSCCM is to impose a constraint on the bond length R_{ON}. When the distance between the two atoms becomes smaller than a given value R_{min}, we invert the projection of the velocities of O and N on the bond in the system of their center of mass. This is equivalent to introducing a hard wall potential between N and O. Figure 2a shows the rate constant $k(E)$ (circles) obtained by PSCCM as a function of the repelling wall position together with the rate constant calculated by the straightforward trajectory simulation shown by the gray line, the width of which indicates the error in the trajectory calculation. The accelerated rate is within the error bar from the trajectory result up to R_{min} = 1.8 Å. The rate constants shown in Figure 2a are also summarized in Table 3a.

The above implementation referred to as implementation 1 introduces an extra potential, and although its nature is different from that of Voter[4−7] (instead of lifting up the bottom of the potential energy well we modify the repulsive part of the potential), the approach is similar in spirit. In implementation 2 we impose a different condition and invert the velocities only when the energy of the ON bond, written as

$$E_{ON} = p_{rel}^2/2\mu_{rel} + V(R_{ON}) \quad (14)$$

with p_{rel} and μ_{rel} being the relative momentum and the reduced mass of the ON bond, respectively, and $V(R_{ON})$, the Morse potential of eq 9, becomes smaller than a given minimal energy E_{min}. The constraint

$$E_{ON} > E_{min} \quad (15)$$

includes momenta, whereas simple boosting potentials[4−8]

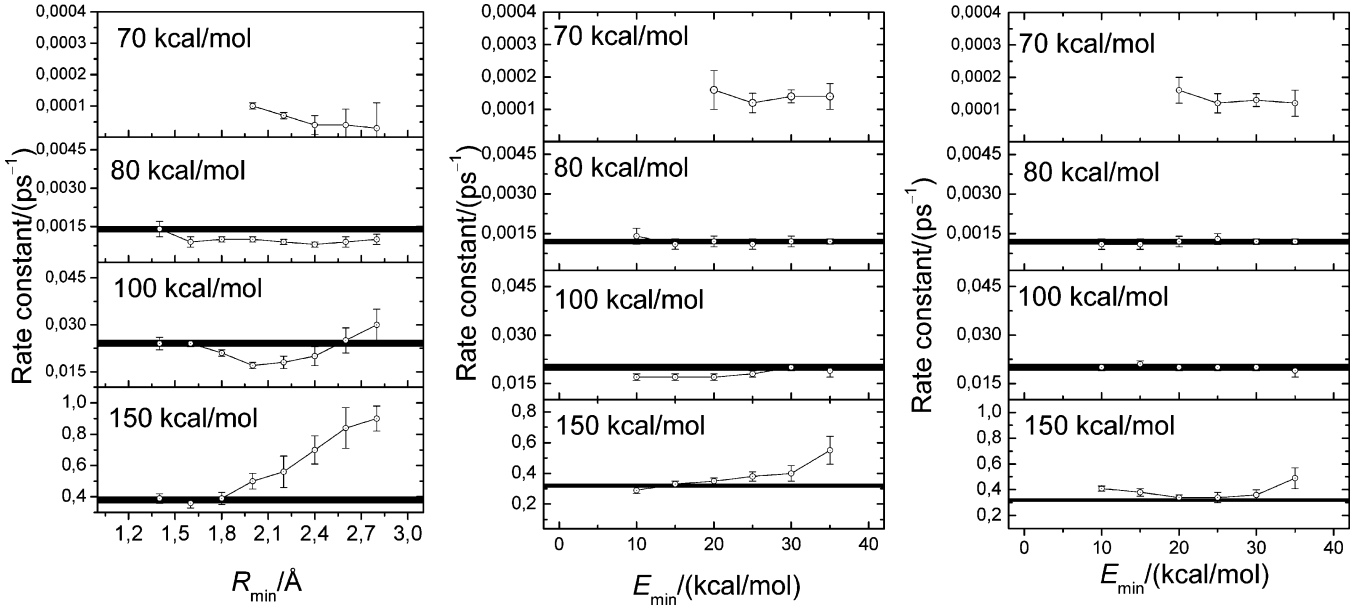

Figure 2. a. The microcanonical rate constant $k(E)$ obtained with the help of PSCM, compared with the result of straightforward trajectory simulation (gray line) for $E = 70$, 80, 100, and 150 kcal/mol as a function of the constraint condition given by R_{min} (the minimum ON bond length) for implementation 1. b. Microcanonical rate constant $k(E)$ obtained with the help of PSCCM compared with the result of straightforward trajectory simulation (gray line) for $E = 70$, 80, 100, and 150 kcal/mol as a function of the constraint condition given by E_{min} (the energy of the diatomic ON fragment) for implementation 2. c. Microcanonical rate constant $k(E)$ obtained with the help of PSCCM compared with the result of straightforward trajectory simulation (gray line) for $E = 70$, 80, 100, and 150 kcal/mol as a function of the constrain condition given by E_{min} (the energy of the diatomic ON fragment) for implementation 3.

depend only on coordinates. Figure 2b and Table 3b show the results of implementation 2 for the rate constants, which are again very close to those of straightforward trajectory simulations, even for the energies E_{min} approaching the dissociation energy of the ON bond. Overall, the performance of implementation 2 is much better than that of implementation 1. However, at the highest energies of this study (100 and 150 kcal/mol) method 2 yields rates a bit smaller than the standard ones, particularly at low E_{min}. We noticed that this behavior could be due to trapping of trajectories in the repulsive part of the ON potential well because on the repulsive part of the ON Morse potential, the energy can be higher than E_{min} and therefore the inversion of O and N velocities can lead to shrinking rather than stretching of the ON bond distance, which may lower the value of the accelerated rate constant.

To prevent this trapping we devised implementation 3. In implementation 3, which is a combination of implementations 1 and 2, the velocity is inverted either when the energy becomes smaller than E_{min} or when the internuclear distance becomes smaller than the equilibrium ON bond length. In this way, we prevent the system from moving to the repulsive part of the potential. Implementation 3 produced the best results, shown in Figure 2c (circles) and Table 3c. Particularly, for the highest energy employed in this study (150 kcal/mol) the method is accurate when $E_{min} \leq 30$ kcal/mol (i.e. up to 70% of the dissociation energy of the molecule). For other energies the method is accurate even for the highest E_{min} of 35 kcal/mol, which is up to 83% of the dissociation energy of the molecule.

Table 3 also shows the computational cost of calculations (CPU time). For example for $E = 80$ kcal/mol straightforward trajectory simulation (TS) required more than 3000 min of CPU time, while implementations 2 and 3 needed only about 100 minutes with approximately 60% of the effort going on running trajectories estimating $k_1^{traj}(E)$ (CPU time in parentheses). The rest was spent on calculating the (Γ_1/Γ) correction factor by random walk.

Figure 3 shows rate constants calculated by PSCCM, straightforward TS, and statistical MCTST. On the scale of the plot the result of PSCCM is indistinguishable from that of straightforward trajectory simulation. In agreement with the predictions of IDDT at high energies, the dynamical calculations produce rates higher than those of statistical MCTST, while at low energies nonstatistical effects are negligible. Accelerated PSCCM allows trajectory simulations for energies unaccessible for straightforward trajectory simulations and pushes the limit of dynamical calculations to low energies where the rate constant reaches its statistical limit.

Therefore PSCCM reproduces nonstatistical effects at high energies. On the other hand, it is most efficient at low energies where trajectory rates are close to statistical, which can be calculated very accurately and efficiently with the help of accelerated MCTST. To compare the PSCCM and MCTST methods at low energies methods Figure 4 shows variation of the rate constant with the position of the dividing surface. MCTST rate has a distinct minimum, which defines the transition state and the actual rate. On the other hand, the PSCCM are much less sensitive to the variations of the dividing surface so that the PSCCM rate constant is in good agreement with the minimized MCTST rate constant. This can be an advantage when variation of the transition state is difficult, for example, if the reaction coordinate cannot be

Table 3. Computational Details and Rate Constants (in ps^{-1}) Obtained in This Study with Implementations 1−3

a. Implementation 1

	$E = 70$ kcal/mol				$E = 80$ kcal/mol				$E = 100$ kcal/mol				$E = 150$ kcal/mol			
	rate			time[a]	rate			time[a]	rate			time[a]	rate			time[a]
traj					0.0012± 0.0001			3348	0.020± 0.001			380	0.32± 0.01			36
PSCCM	$k^{traj}(E)$	$k_1^{traj}(E)$	Γ_1/Γ		$k^{traj}(E)$	$k_1^{traj}(E)$	$\Gamma a_1/\Gamma$		$k^{traj}(E)$	$k_1^{traj}(E)$	Γ_1/Γ		$k^{traj}(E)$	$k_1^{traj}(E)$	Γ_1/Γ	
R_{min}[b]																
1.4					0.0014± 0.0003	0.0020	0.70	121 (119)	0.024± 0.002	0.033	0.72	114 (112)	0.39± 0.03	0.49	0.78	43 (42)
1.6					0.0009± 0.0002	0.0045	0.21	114 (108)	0.024± 0.001	0.085	0.29	110 (106)	0.36± 0.03	0.77	0.47	31 (29)
1.8					0.0010± 0.0001	0.023	0.041	107 (101)	0.021± 0.001	0.22	0.093	104 (98)	0.39± 0.04	1.46	0.27	23 (19)
2.0	0.00010± 0.00001	0.029	0.0032	1971 (1171)	0.0010± 0.0001	0.12	0.0087	100 (71)	0.017± 0.001	0.51	0.034	68 (53)	0.50± 0.05	2.95	0.17	20 (12)
2.2	0.00007± 0.00001	0.11	0.00058	1759 (1194)	0.0009± 0.0001	0.36	0.0025	105 (59)	0.018± 0.002	1.11	0.016	42 (27)	0.56± 0.10	4.97	0.11	16 (8)
2.4	0.00004± 0.00003	0.30	0.00015	1980 (1151)	0.0008± 0.0001	0.74	0.0011	85 (36)	0.020± 0.003	2.09	0.0094	40 (15)	0.70± 0.09	8.90	0.079	15 (5)
2.6	0.00004± 0.00005	0.64	0.000060	1575 (1104)	0.0009± 0.0002	1.43	0.00060	79 (22)	0.025± 0.004	4.17	0.0061	44 (10)	0.84± 0.13	15.4	0.054	13 (3)
2.8	0.00003± 0.00008	1.24	0.000028	1762 (1103)	0.0010± 0.0002	2.80	0.00035	105 (12)	0.030± 0.005	7.34	0.0041	95 (6)	0.90± 0.08	27.1	0.033	20 (3)

b. Implementation 2

	$E = 70$ kcal/mol				$E = 80$ kcal/mol				$E = 100$ kcal/mol				$E = 150$ kcal/mol			
	rate			time[a]	rate			time[a]	rate			time[a]	rate			time[a]
traj					0.0012± 0.0001			3348	0.020± 0.001			380	0.32± 0.01			36
PSCCM	$k^{traj}(E)$	$k_1^{traj}(E)$	Γ_1/Γ		$k^{traj}(E)$	$k_1^{traj}(E)$	Γ_1/Γ		$k^{traj}(E)$	$k_1^{traj}(E)$	Γ_1/Γ		$k^{traj}(E)$	$k_1^{traj}(E)$	Γ_1/Γ	
E_{min}[c]																
10					0.0014± 0.0003	0.0072	0.19	143 (132)	0.017± 0.001	0.06	0.30	105 (92)	0.29± 0.02	0.56	0.52	59 (47)
15					0.0011± 0.0002	0.014	0.078	150 (130)	0.017± 0.001	0.10	0.16	106 (83)	0.33± 0.02	0.86	0.38	45 (33)
20	0.00016± 0.00006	0.010	0.016	175 (152)	0.0012± 0.0002	0.037	0.033	160 (125)	0.017± 0.001	0.19	0.088	93 (78)	0.35± 0.02	1.15	0.30	59 (31)
25	0.00012±0.00003	0.022	0.0055	181 (135)	0.0011± 0.0002	0.081	0.013	144 (113)	0.018± 0.001	0.39	0.048	67 (47)	0.38± 0.03	1.82	0.21	31 (18)
30	0.00014± 0.00002	0.077	0.0018	142 (100)	0.0012± 0.0002	0.22	0.0053	126 (70)	0.020± 0.001	0.76	0.026	59 (31)	0.40± 0.05	2.67	0.15	26 (14)
35	0.00014± 0.00004	0.25	0.00055	195 (92)	0.0012± 0.0001	0.55	0.0022	132 (51)	0.019± 0.002	1.34	0.014	37 (16)	0.55± 0.09	5.04	0.11	38 (6)

c. Implementation 3

	$E = 70$ kcal/mol				$E = 80$ kcal/mol				$E = 100$ kcal/mol				$E = 150$ kcal/mol			
	rate			time[a]	rate			time[a]	rate			time[a]	rate			time[a]
traj					0.0012± 0.0001			3348	0.020± 0.001			380	0.32± 0.01			36
PSCCM	$k^{traj}(E)$	$k_1^{traj}(E)$	Γ_1/Γ		$k^{traj}(E)$	$k_1^{traj}(E)$	Γ_1/Γ		$k^{traj}(E)$	$k_1^{traj}(E)$	Γ_1/Γ		$k^{traj}(E)$	$k_1^{traj}(E)$	Γ_1/Γ	
E_{min}[b]																
10					0.0011± 0.0002	0.0074	0.15	138 (128)	0.020± 0.001	0.078	0.25	100 (88)	0.41± 0.02	0.88	0.46	43 (32)
15					0.0011± 0.0002	0.016	0.068	145 (127)	0.021± 0.001	0.15	0.14	104 (81)	0.38± 0.03	1.08	0.35	42 (30)
20	0.00016±0.00004	0.0098	0.016	170 (148)	0.0012± 0.0002	0.041	0.030	154 (120)	0.020± 0.001	0.24	0.080	92 (77)	0.34± 0.02	1.30	0.26	39 (25)
25	0.00012± 0.00003	0.022	0.0055	180 (132)	0.0013± 0.0002	0.11	0.012	136 (109)	0.020± 0.001	0.44	0.045	63 (45)	0.34± 0.04	1.70	0.20	25 (13)
30	0.00013± 0.00002	0.073	0.0018	138 (99)	0.0012± 0.0001	0.23	0.0051	99 (59)	0.020± 0.001	0.80	0.025	55 (28)	0.36± 0.04	2.50	0.14	24 (15)
35	0.00012± 0.00004	0.23	0.00053	167 (84)	0.0012± 0.0001	0.55	0.0021	124 (53)	0.019± 0.002	1.38	0.014	36 (16)	0.49± 0.08	5.04	0.098	17 (7)

[a] Total CPU time (in min). In the PSCCM calculations the time is the sum of CPU times for the calculation of $k_1^{traj}(E)$ (in parentheses) and Γ_1/Γ. [b] E_{min} in kcal/mol. [c] R_{min} in Å

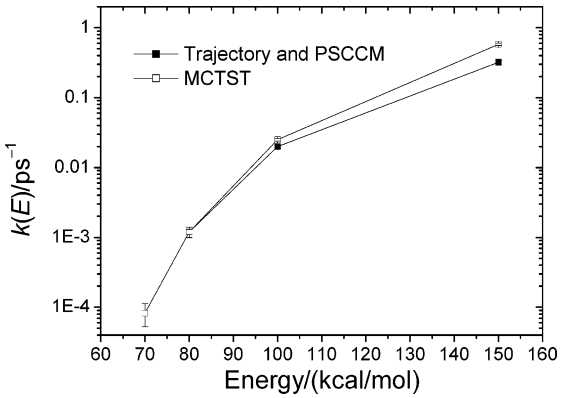

Figure 3. Rate constants $k(E)$ calculated by standard straightforward trajectory simulation (black square) [PSCCM (method 3 E_{min}=30 kcal/mol) is indistinguishable from trajectory simulation] and the statistical Monte Carlo Transition State Theory (open square). Dynamical PSCCM calculation shows that nonstatistical effects are absent at low energies (70 and 80 kcal/mol), thereby confirming the predictions of the Intramolecular Dynamics Diffusional Theory.

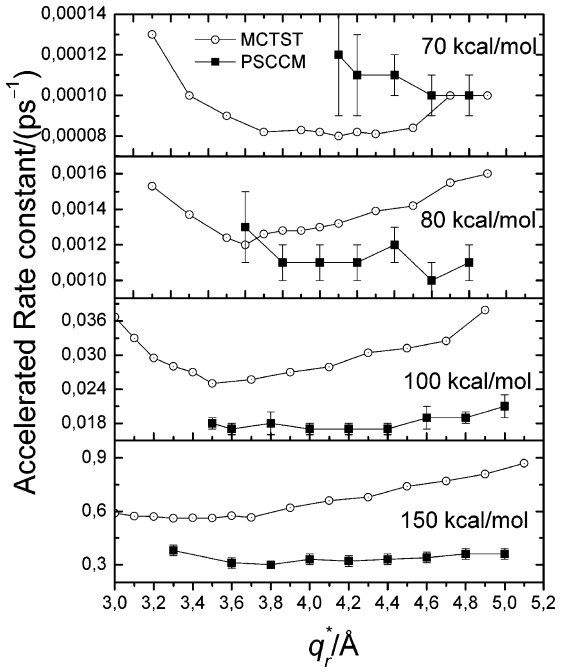

Figure 4. Variations of the rate constants obtained by MCTST (open circles) and PSCCM (black squares) with the position of the dividing surface. The actual position minimizes MCTST rate. The PSCCM rate is less sensitive to the position of the dividing surface.

defined as easily as in the current case of simple bond fission. PSCCM might be able to produce correct results even without a careful choice of the dividing surface. Of course, some general principles of defining constraints should be met. First, the allowed phase space volume should be far enough from the dividing surface to include all nonstatistical effects. On the other hand, the allowed phase space should be made as small as possible in order to make PSCCM numerically efficient.

4. Summary and Conclusions

In this article we propose a new version of accelerated dynamics based on phase space constraints rather then previously suggested boosting potentials.[4−8] We demonstrated that the approach speeds up trajectory simulations with no loss of accuracy. For example as Table 3a−d shows, for $E = 80$ kcal/mol the CPU time required by PSCCM is more than an order of magnitude smaller than that of straightforward trajectory simulation. For $E = 70$ kcal/mol straightforward trajectory simulation was not feasible, but simple extrapolation of CPU time suggests acceleration by more then 2 orders of magnitude.

The method of PSCCM is based on the Intramolecular Dynamics Diffusional Theory. On the other hand, accelerated PSCCM helped to demonstrate that nonstatistical effects at lower energies become less important so that the dynamical simulation simply reproduces the statistical MCTST rate (see Figure 5). Previously this prediction of IDDT could not be directly verified without accelerating the dynamics. Therefore PSCCM fills the gap between trajectory simulations at high energies and MCTST at low energies. Like any other version of accelerated dynamics Phase Space Constrained Classical Mechanics should be used for energies low enough for straightforward trajectory simulations to be time-consuming but high enough for nonstatistical effects to be important for IVR limited intrinsic non-RRKM reactions. At low energies rates are statistical and therefore can (and should) be easily estimated by the accelerated Monte Carlo Transition State Theory.[22] However, at low energies PSCCM is still useful since, as it is shown at Figure 4, PSCCM is less sensitive to variations of the dividing surface. Therefore, PSCCM, which could be even faster than accelerated MCTST at low energies, can be used when the dividing surface is difficult to define.

Acknowledgment. We thank "Centro de Supercomputación de Galicia" (CESGA) for the use of their facilities. E.M.-N. acknowledges Ministerio de Ciencia y Tecnología of Spain for financial support through "Ramón y Cajal" program. D.S. acknowledges the support from UK EPSRC. We also would like to thank Prof. M. S. Child for his useful comments.

Appendix

Some Details of the Calculations. The trajectories were integrated using the Runge−Kutta algorithm with a fixed step size of 0.05 fs, which is enough to ensure an excellent energy conservation: the maximum energy difference along the trajectories is 3×10^{-5}%. For the highest energies considered in this study (100 and 150 kcal/mol), the trajectories were followed until R_{ON} reaches the dividing surface (see above) or 5 ps elapsed. For the lowest energies (70 and 80 kcal) the maximum time for a trajectory was 20 ps. Ensembles of 1000 trajectories were employed in all cases (for standard and PSCCM calculations) except for the standard trajectory calculations at 80 kcal/mol, for which we needed 3000 trajectories to get the same statistics as in the accelerated computations. Two different types of initial conditions were used in the present study for standard and

PSCCM calculations: efficient microcanonical sampling (EMS)[11] and Metropolis sampling.[19] The microcanonical rate constants obtained from standard trajectory simulations with both initialization methods (EMS and Metropolis) are very similar. For both EMS and Metroplis we used warm-up random walks of 500 000 steps and walks of 10 000 steps between trajectories. Additionally, the maximum displacement for the atoms in each step of the random walk in the EMS was 0.07 Å. For the Metropolis sampling the maximum displacements for the Cartesian coordinates and momenta were both 0.1 (in Å and (kcal/mol×amu),$^{1/2}$ respectively). In Metropolis sampling the probability for acceptance/rejection of a given point along the walk is given by

$$P = \begin{cases} \epsilon/\{\epsilon^2 + [E - H(q,p)]\} & \text{for } |E - H| < E_{\text{limit}} \\ 0 & \text{otherwise} \end{cases} \quad (16)$$

In the present work we used $\epsilon = 10$ and $E_{\text{limit}} = 10$ kcal/mol. Acceptance/rejection ratios close to 0.5 were achieved in all cases. The same random walk was employed both for choosing the initial conditions of trajectory simulation and for calculating the statistical MCTST rates.

References

(1) Shelley, J. C.; Shelley, M. Y.; Reeder, R. C.; Bandyopadhyay S.; Klein M. L. *J. Phys. Chem B* **2001**, *105*, 4464.

(2) Nielsen, S. O.; Lopez, C. F.; Srinivas, G.; Klein, M. L. *J. Chem. Phys.* **2003**, *119*, 7043.

(3) Chandler, D. *J. Chem. Phys*. **1978**, *68*, 2959. Montgomery, J. A., Jr.; Chandler, D.; Berne, B. J. *J. Chem. Phys*. **1979**, *70*, 4056.

(4) Voter, A. F. *Phys. Rev. B* **1998**, *57*, 13985.

(5) Voter, A. F. *J. Chem. Phys.* **1997**, *106*, 4665.

(6) Voter, A. F. *Phys. Rev. Lett.* **1997**, *78*, 3908.

(7) Montalenti, F.; Sørensen, M. R.; Voter, A. F. *Phys. Rev. Lett.* **2001**, *87*, 126101.

(8) Voter, A. F.; Montalenti, F.; Germann, T. G. *Annu. Rev. Mater. Res.* **2002**, *32*, 3219.

(9) Grimmelmann, E. K.; Tully, J. C.; Helfand, E. *J. Chem. Phys.* **1981**, *74*, 5300.

(10) (a) Brady, J. W.; Doll, J. D.; Thompson, D. L. *J. Chem. Phys.* **1980**, *73*, 2767. (b) Brady, J. W.; Doll, J. D.; Thompson, D. L. *J. Chem. Phys.* **1981**, *74*, 1026−1028. (c) Viswanathan, R.; Thompson, D. L.; Raff, L. M. *J. Chem. Phys.* **1984**, *80*, 4230. (d) NoorBatcha, I.; Raff, L. M.; Thompson, D. L. *J. Chem. Phys.* **1986**, *84*, 4341. (e) Rice, B. M.; Raff, L. M.; Thompson, D. L. *J. Chem. Phys.* **1986**, *85*, 4392. (f) Gai, H.; Thompson, D. L.; Raff, L. M. *J. Chem. Phys.* **1988**, *88*, 156. (g) Agrawal, P. M.; Thompson, D. L.; Raff, L. M. *J. Chem. Phys.* **1988**, *89*, 741. (h) Agrawal, P. M.; Thompson, D. L.; Raff, L. M. *J. Chem. Phys.* **1990**, *92*, 1069. (i) Sewell, T. D.; Thompson, D. L. *J. Chem. Phys.* **1990**, *93*, 4077. (j) Schranz, H. W.; Raff, L. M.; Thompson, D. L. *J. Chem. Phys.* **1991**, *94*, 4219. (k) Schranz, H. W.; Raff, L. M.; Thompson, D. L. *Chem. Phys. Lett.* **1991**, *182*, 455. (l) Sewell, T. D.; Schranz, H. W.; Thompson, D. L.; Raff, L. M. *J. Chem. Phys*. **1991**, *95*, 8089. (m) Sorescu, D. C.; Thompson, D. L.; Raff, L. M. *J. Chem. Phys*. **1994**, *101*, 3729. (n) Rice, B. M.; Adams, G. F.; Page, M.; Thompson, D. L. *J. Phys. Chem.* **1995**, *99*, 5016. (o) Chambers, C. C.; Thompson, D. L. *J. Phys. Chem.* **1995**, *99*, 15881.

(11) Sewell, T. D.; Thompson, D. L. *Int. J. Mod. Phys. B* **1997**, *11*, 1067.

(12) Sørensen, M. R.; Voter, A. F. *J. Chem. Phys*. **2000**, *112*, 9599.

(13) Shalashilin, D. V.; Thompson, D. L. *J. Chem. Phys.* **1996**, *105*, 1833.

(14) Guo, Y.; Shalashilin, D. V.; Krouse, J. A.; Thompson, D. L. *J. Chem. Phys.* **1999**, *110*, 5514; **1999**, *110*, 5521.

(15) Shalashilin, D. V.; Thompson, D. L. *J. Chem. Phys.* **1997**, *107*, 6204.

(16) Shalashilin, D. V.; Thompson, D. L. In *Highly Excited Molecules*; ACS Symposium Series; American Chemical Society: Washington, DC, 1997; Vol. 678, p 81.

(17) Gray, S. K.; Rice S. A.; Davis, M. J. *J. Phys. Chem* **1986**, *90*, 3470.

(18) Doll, J. D. *J. Chem. Phys.* **1981**, *74*, 1074.

(19) Metropolis, N.; Rosenbluth, A. W.; Rosenbluth, M. N.; Teller, A. H.; Teller, E. J. *J. Chem. Phys.* **1953**, *21*, 1087.

(20) Bunker, D. L.; Hase W. L. *J. Chem. Phys*. **1973**, *59*, 4621.

(21) Hase, W. L. *J. Chem. Phys.* **1978**, *69*, 4711.

(22) Shalashilin, D. V.; Thompson, D. L. *J. Phys. Chem. A* **1997**, *101*, 961.

(23) Bowman, J. M.; Gazdy, B.; Sun, O. *J. Chem. Phys.* **1989**, *91*, 2859.

(24) Miller, W. H.; Hase, W. L.; Darling, C. L. *J. Chem. Phys.* **1989**, *91*, 2863.

(25) Sewell, T. D.; Thompson, D. L.; Gezelter, J. D.; Miller, W. H. *Chem. Phys. Lett.* **1992**, *193*, 512.

(26) Peslherbe, G. H.; Hase, W. L. *J. Chem. Phys.* **1994**, *100*, 1179.

(27) Martínez-Núñez, E.; Vázquez, S. A. *J. Chem. Phys*. **1998**, *109*, 8907.

CT060042Z